Optical fiber-based single-shot picosecond transient absorption spectroscopy

Andrew R. Cook[a] and Yuzhen Shen
Department of Chemistry, Brookhaven National Laboratory, Upton, New York 11973, USA

(Received 27 January 2009; accepted 29 May 2009; published online 17 July 2009)

A new type of single-shot transient absorption apparatus is described based on a bundle of optical fibers. The bundle contains 100 fibers of different lengths, each successively giving ~15 ps longer optical delay. Data are collected by imaging light from the exit of the bundle into a sample where it is overlapped with an electron pulse or laser excitation pulse, followed by imaging onto a charge coupled device (CCD) detector where the intensity of light from each fiber is measured simultaneously. Application to both ultrafast pump-probe spectroscopy and pulse radiolysis is demonstrated. For pulse radiolysis, the prototype bundle provides the ability to collect data with a time resolution limited only by the electron pulse width of 7–10 ps, over a total single-shot time window of ~1.5 ns. Tunable probe light is obtained from a titanium-sapphire laser and an optical parametric amplifier. Corrections are made to remove the fiber-to-fiber variations in signal magnitude due to the spatial overlap of the electron beam and probe image. High quality data can be collected over most of the sensitivity range of the CCD camera detectors. The single-shot instrument is valuable for measurement of samples that are only available in very limited quantities, are too viscous to flow, or are rigid. It is therefore excellent in applications, such as picosecond pulse radiolysis, where the thousands of pulses per kinetic trace typical in classical pump-probe experiments can damage the sample before useful results could be obtained. © *2009 American Institute of Physics.* [DOI: 10.1063/1.3156048]

I. INTRODUCTION

Ultrafast laser pump-probe transient absorption spectroscopy is a standard way to measure reaction dynamics on picosecond and femtosecond time scales.[1] In such experiments, a variably delayed laser probe pulse interrogates a sample at different times relative to an excitation pulse. By taking absorption measurements using different positions along a mechanical optical delay line, kinetic data are collected in a serial fashion. Each excitation pulse yields transient absorption at a single delay time. Many measurements are averaged at each delay time. This technique is especially powerful with modern high-repetition rate lasers, making data collection rapid. Complete kinetic traces are typically measured using 10^4–10^6 laser pulses, depending on the desired signal-to-noise (S/N) ratio and number of time points measured. Moving the delay line can often represent the greatest part of the time required to collect a transient.

While quite powerful, this method is not ideal in all situations. Low repetition rate systems are required in certain circumstances, which can greatly increase the amount of time required to collect acceptable S/N data from a few minutes to significant fractions of an hour or more. This problem can be exacerbated by larger excitation pulse fluctuations inherent to many such systems, greatly increasing noise between different time points. Serious problems with samples can also occur including excitation-induced damage, irreversible reactions, and product buildup. These can be mitigated in some cases by flowing a large volume of the sample so that each pulse interrogates fresh solution. In addition to the large amount of waste generated by using flow systems, circumstances exist where it is not possible to flow certain samples. For example, many custom synthesized compounds are costly and time consuming to make, thus are impractical to produce in the quantities required for even very small flow systems. Other samples are too viscous to flow or are solids. For all such samples, conventional pump-probe techniques are usually not viable.

It is therefore desirable to record complete transient absorption kinetic traces ideally with a single excitation pulse, or by averaging very small numbers of traces to achieve acceptable S/N. Such single-shot methods were first explored shortly after the advent of picosecond lasers.[2,3] These early techniques, which employed spatial encoding of temporal information across the probe beam, have greatly matured in a number of laboratories, taking full advantage of the time resolution afforded by femtosecond lasers. Relatively simple approaches have taken advantage of the different delay times that occur across the interaction region of pump and probe beams when overlapped at an angle at a given wavelength.[4–6] This method has been extended with the addition of a spectrally broad probe pulse for the collection of time-resolved absorption spectra as well.[7] A more complicated example uses a pair of crossed stair-stepped transparent echelons in the probe beam to introduce delay to different portions of the probe beam.[8–10] These techniques emphasize high temporal resolution, but are only able to provide infor-

[a]Author to whom correspondence should be addressed. Electronic mail: acook@bnl.gov.

mation within a few tens of picoseconds time window. A different type of single-shot method based on frequency encoding of temporal information has also been demonstrated. This method uses a stretched femtosecond laser pulse in which the different wavelengths have been dispersed in time. When crossed with an excitation pulse in the sample, transient absorption information is imprinted across the spectrum of the "chirped" probe pulse and read out using a spectrograph and array detector.[11,12] This technique has been demonstrated with a larger time window, up to 160 ps, while presenting oscillations in the first few picoseconds that require additional analysis and which are sensitive to dynamical spectral shifts.[12] Streak cameras have also been employed in single-shot instruments[13,14] that obtained 30–50 ps rise times, but must trade off time resolution with dynamic range because of distortions due to blooming on the detector at high probe light intensities. Blooming can also be caused by short bursts of light from fluorescence and Cerenkov radiation. A new type of higher dynamic range streak camera (10^3:1 for 5 ps time resolution, 10^4:1 for 100 ps) has recently been employed to reduce difficulties due to blooming.[15,16]

Single-shot transient absorption is highly desirable for pulse radiolysis. The Brookhaven National Laboratory Laser Electron Accelerator Facility[17] (LEAF) produces 7–10 ps electron pulses, which are well synchronized with femtosecond laser pulses. This allows for an experiment analogous to the pump-probe technique described above. In this instance, chemistry is initiated not by optical excitation but with electron pulses. Transient absorption is similarly recorded with a variably delayed optical probe pulse. However, pulse radiolysis often causes unacceptable degradation of the sample and accumulation of undesired products through repetitive pulsing. The 10 Hz repetition rate at LEAF also leads to long data acquisition times causing the measurement to be subject to instrumental drift. To avoid such problems, we have developed a novel type of spatially encoded single-shot transient absorption apparatus based on a bundle of varying length optical fibers. This approach is generally applicable to both pump-probe and electron pulse-laser probe experiments. At LEAF, it provides time resolution limited only by the electron pulse width, coupled with the ability to have arbitrary single-shot time windows. Time windows that can extend to many nanoseconds while preserving high time resolution are important because it makes it possible to adequately overlap and combine single-shot data with those collected on longer time scales using flash lamps, high bandwidth transient digitizers, and fast photodetectors,[17] while avoiding artifacts and distortions common to such fast detectors at short times.[18] Additional benefits of the new single-shot system include the ability to easily and widely tune the probe wavelength, and to interrogate samples with total volumes as small as 100 μl. These capabilities enable new experiments at LEAF that were previously not possible due to very limited sample availability and/or high viscosity. A description of this new experimental system follows, along with notes on its calibration and applications.

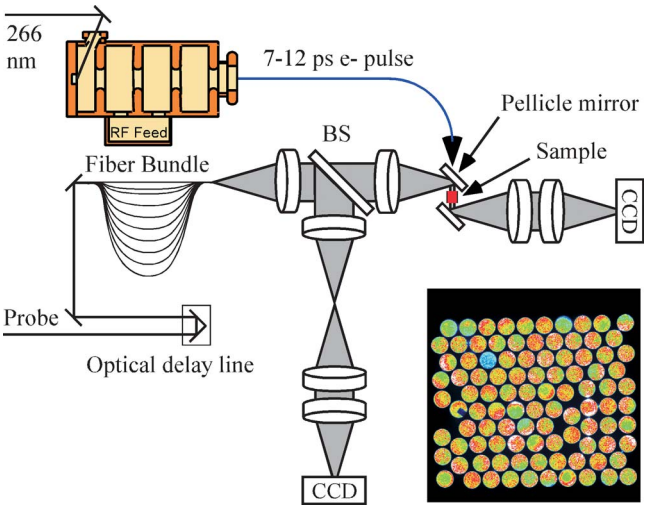

FIG. 1. (Color online) Schematic layout of the fiber-based single-shot transient absorption apparatus. The inset is an image of the fiber bundle collected by the signal CCD camera after a single laser probe pulse, colored by the light intensity recorded by each CCD pixel (details in text).

II. DESCRIPTION

This apparatus was designed to measure chemical reaction dynamics resulting from optical excitation, pulse radiolysis, or a combination of the two. A schematic layout of the optical fiber-based single-shot (OFSS) transient absorption apparatus is shown in Fig. 1. The laser and electron sources for this experiment have been described previously.[17] Briefly, 800 nm, 100 fs pulses from a Ti:sapphire amplifier at 10 Hz are split into two beams. The first beam is frequency tripled to 266 nm, and used to pump a photocathode in the LEAF accelerator to produce 7–10 ps electron pulses. The other beam is either used directly or to pump an optical parametric amplifier (OPA) (Light Conversion TOPAS-4/800-FS) that provides remotely tunable probe light from 240–2600 nm, although only a subset of that range is used in this experiment as described below. As in a standard pump-probe or electron pulse-laser probe experiment, the probe first traverses a mechanical delay line (Parker 406T13LXR with 1700 mm travel and 1 μm accuracy, Gemini GV-U6E driver, 6K4 controller) to change the relative excitation—probe delay time. For OFSS, this allows for adjustment of the entire probe time window with respect the electron pulse. The probe is then injected into the fiber bundle. The light exiting the bundle is split into signal and reference arms, where it is ultimately imaged onto charge coupled device (CCD) cameras. The sample is placed in one arm at a focal point of the fiber bundle image relay system, and crossed collinearly with either an electron pulse, or a laser excitation pulse (not shown).

The key new concept in this apparatus is the use of different length optical fibers in a bundle to provide various optical delays, rather than using a moving delay line. The prototype fiber bundle currently in use was custom made by Fiberguide Industries, Inc. using 200/220 μm diameter core/clad step-index silica fiber (SuperguideG, HighOH). For the first bundle, fiber with a numerical aperture (NA) of 0.22 was chosen, as the manufacturer was concerned with the

brittleness of lower NA fiber leading to an increased chance of broken fibers in the final product. There are a total of 100 fibers in the bundle, each cleaved to be ~3 mm different in length, with the shortest being ~1.4 m long. At 800 nm, this gives about a 15 ps delay for each successive fiber, and a total single-shot time window of ~1.5 ns. The buffer material was stripped from both ends of each fiber so that they can be placed as close together as possible in the bundle ferrules, and the excess fiber was simply coiled up in a box in between. No attempt was made to order the fibers by length in either end of the bundle. The remaining thin, 10 μm, cladding on the fibers allows them to be closely packed, making for a smaller image in the sample and minimizing wasted pixels on the detectors. The diameter of the fiber was chosen, as were the details of the optical system, to balance the objective of producing a small image in the sample with that of using the maximum detector area. The fiber bundle entrance is 2.8 mm in diameter. To maximize the use of the square detector, the fibers in the exit end of the bundle were arranged in a roughly square configuration, 1.9×2.3 mm^2 in size.

Even with the use of a reference beam, it was found to be advantageous to have a fairly equal amount of light in each fiber. This allows for the maximum amount of probe light to be used without saturating the detectors, and avoids greater noise from fibers that are more poorly illuminated. Initial tests to provide uniform illumination of the fibers were done using a Galilean telescope to expand the laser beam so that only the central and more flattop portion of the beam was used. Due to mode imperfections present in 10 Hz sources, and the long distance the beam is transported from the laser (~10 m) necessitated by the radiation safety considerations in LEAF, it was found that even with this expansion, shot-to-shot irregularities in the mode were apparent in the illumination of the fibers. A better system was implemented using a pair of holographic diffusers (Edmund Optics, NT54-496: 20° circular, NT47-995: 5° circular) to homogenize the beam right before the fiber bundle, giving relatively even amounts of light injected into all fibers on a shot-to-shot basis. The 20° diffuser was placed ~5.5 cm from the bundle entrance, followed immediately by a 25.4 mm focal length lens to reduce the size of the diffuse spot. The 5° diffuser was subsequently placed ~0.5 cm from the bundle. The brightest part of the final diffuse spot is approximately five times the fiber bundle diameter. An added benefit of the diffusers is that they produce a spatially incoherent light beam, which helps to reduce the speckle present at the output end of the bundle. The light intensity was adjusted by a combination of the 5° diffuser position and neutral density filters before injection to produce an average signal between 2% and 50% of the maximum on the CCD camera. The actual injected light intensity was not measured, as it depends on the wavelength and the amount of light that the OPA produces; however one can estimate from the signal levels on the cameras and the optical system described below that it lies in the range of tens to hundreds of nanojoules/pulse.

Light exiting the fiber bundle is subsequently imaged with the optical system shown in Fig. 1. All of the lenses employed are 50.4 mm diameter achromats, with antireflection coatings (ThorLabs and CVI). The achromats are optimized for 650–1050 nm. While not ideal, they have been used down to 540 nm. For better performance, different optics will be substituted for wavelengths below 650 nm in the future. Light exiting the bundle is approximately collimated with a 400 mm focal length lens. Note that with a NA =0.22, an ~90 mm diameter lens of this focal length is necessary to capture all of the light exiting the bundle. The smaller diameter optics employed were a compromise made to maintain a manageable optical system with sufficient space around the sample and image sizes at the sample and detectors. The resulting loss of light and slightly poorer focusing ability have not been significant issues. The light is then divided into equivalent reference and signal arms by a beam splitter (BS). It was found that a dielectric 40% BS centered at 800 nm (CVI, BS1–800, 76.2 mm diameter), while not ideal, provides sufficient light in the reference arm for a wide range of wavelengths, as tested from 540 to 950 nm. This will later be improved with either a series of interchangeable BSs with broader band coatings, or a single one with a very broadband metallic coating. It was found necessary to use a 12.7 mm thick BS to avoid ghost images from the backside, as the antireflection coating was insufficient. The optics in each arm have focal lengths of 200, 200, and 2000 mm successively. These give a smaller image in the sample ($\sim 1 \times 1.2$ mm), while still providing a long enough distance from the lens to easily fold the beam as shown around the sample. The first fold mirror is a small protected silver coated pellicle (National Photocolor, 0.5″-ETP-LQ) to allow the electron beam to pass through with minimal scattering to produce the smallest possible electron beam spot diameter, and to overlap collinearly with the probe in the sample. The pellicle needs to be replaced occasionally due to slow accumulation of damage caused by the electron beam. For experiments with optical excitation, the same setup is used, but the pump beam is brought in at a slight angle. Due to the radiation present when the electron beam is in use, selected lenses and mirror mounts are motorized to allow for remote alignment and focusing. The CCD detectors (Andor Technology, 512×512 pixel backilluminated DV412-BV-990, cooled to −20 °C, sensitive 200–1050 nm), which have a 12.5×12.5 mm active area, are nearly filled with the image of the fiber bundle to maximize the number of pixels in each individual fiber spot. Neutral density filters with an optical density of 1.0 are placed in front of each camera to reduce ambient and scattered light. The inset in Fig. 1 shows a typical (false colored) image recorded by one of the CCD cameras after a single 800 nm probe pulse. The colors represent different light intensities recorded at each pixel, and the larger round spots are images of each individual fiber. The variation in colors within a fiber spot is speckle caused by modal noise,[19] and corresponds to an ~30% range of pixel intensities from the average. As can be seen, the image recorded by the cameras is quite sharp. The average light level fiber to fiber is fairly uniform, within 10%. A critical requirement for the imaging system is to avoid crosstalk between adjacent fibers. To quantify crosstalk, light was injected into one fiber at a time using a 200 μm pinhole. The

output images indicate that the light is substantially confined to a single fiber spot, with the light in other areas being three to four orders of magnitude less intense. Finally, the effects of any crosstalk are minimized by the random arrangement of the fibers.[20]

III. CALIBRATION

Before this apparatus could be used, the relative delays between the fibers needed to be calibrated. The inset of Fig. 1 shows a sample image collected and processed using LABVIEW and the Vision Development Toolkit (both from National Instruments). The light intensity from each fiber is defined in the analysis software by drawing a circle around the image from each fiber within the images from the cameras, and summing the intensities from the roughly 1200 pixels within that circle. The calibration of the time axis is obtained using the electronic optical Kerr effect[21] (OKE) in fused silica. Calibration experiments were performed using the 800 nm fundamental of the Ti:sapphire laser. The calibration is subsequently adjusted for different probe colors based on the change in the index of refraction in the fused silica fibers. For these measurements, a gate pulse was split off before the optical delay line and spatially overlapped with the probe in a 2 mm thick fused silica window at a small angle. Crossed polarizers were inserted into the probe beam on either side of the sample, and the excitation beam was rotated with a half-wave plate to 45° relative to the probe. In fused silica, the gate pulse induces birefringence primarily through the fast electronic Kerr effect, which only lasts as long as the gate pulse duration. When the gate pulse is overlapped in time with light from one of the fibers, the induced birefringence causes rotation of the probe light polarization, allowing transmission through the analyzing polarizer and observation on the CCD detector. Without the gate pulse, no light reaches the detector. Moving the delay line and observing the position when each fiber spot appeared in the camera image thus allowed determination of the relative delay of each fiber. It was found that the delays were within a few picoseconds to those expected for the intended lengths of the fibers, giving an average fiber-to-fiber delay just under 15 ps and a total time window of 1.472 ns at 800 nm.

This experiment also gives a measure of the instrument response time. If the ~100 fs gate pulse is much narrower than the probe pulse, the cross-correlation function gives an accurate representation of the probe pulse profile. Because of the bandwidth of the 100 fs probe pulses, group velocity dispersion (GVD) causes broadening as a function of length of the fibers.[22] For the shortest fiber (~137 cm), a transform-limited probe pulse is expected to be broadened to ~1.4 ps. The OKE measurements indicate that the pulse durations from shortest and longest fibers are 1.6 and 1.9 ps, respectively. By simply adjusting the length of the laser amplifier pulse compressor, it is possible to precompensate for some of the GVD in the fibers. With little effort, it was possible to shorten the OKE signal 10%–90% rise time from the shortest fiber to 0.5 ps. The minimum pulse width is most likely limited by higher order GVD. While precompensation is easy to do for 800 nm light, OPA generated probes would require additional effort. For pulse radiolysis experiments, shortening the probe pulse duration is not necessary, as our time resolution is limited by the electron pulse width of 7–10 ps.

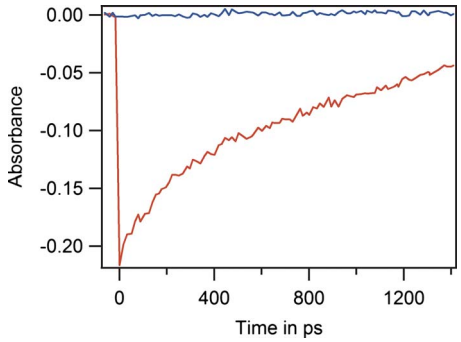

FIG. 2. (Color online) Transient absorption bleach data collected at 800 nm for IR140 laser dye in acetone, collected with a single laser excitation pulse (red, lower trace). Also shown is a single base line shot collected without excitation (blue, upper trace).

IV. RESULTS

A. Single-shot laser pump-probe detection

The first demonstration of the capability of this apparatus used only the signal CCD camera to record transient absorption kinetics following 100 fs optical excitation. As above, both pump and probe were 800 nm, with the excitation beam overlapping the probe image in the sample at a small angle, with parallel polarization. The sample used in this study was IR140 (Lambda Physik) laser dye dissolved in acetone, for which an excited-state lifetime of ~1.2 ns was reported with near infrared (IR) excitation.[23] A sample with an absorption of ~40% for the pump was prepared in a fused silica cell having a 1 mm path length. The pump beam (initially ~500 μJ/pulse) was spatially filtered and then expanded to greater than 20 times the bundle image size before overlapping with the probe, such that the pump intensity that overlapped each fiber spot in the image was fairly uniform as determined by variations in the fiber-to-fiber signal magnitude. A sample cell with high quality antireflection coated windows was made to reduce scattered excitation light and eliminate ghost images. The probe light level was adjusted to about half the saturation level of the detector, and a 40 ms CCD exposure time ensured that only one pulse of the 10 Hz laser was used. Data were collected using a series of two probe images, one with and one without the pump. Another image with no probe determined the camera background level, which was subtracted from both images. A small amount of fluorescence was nearly uniformly distributed across the detector, and was sufficiently small to be neglected. Figure 2 shows the resulting decay of the transient absorption bleach recorded with a single laser excitation pulse, with a decay rate in good agreement with the previously published results. Data with similar S/N collected with a variably delayed probe pulse with our laser system take many thousands of shots and 20–30 min to collect. This clearly demonstrates the noise elimination power of single-

shot techniques by removing the effect of pump shot-to-shot fluctuations. An additional improvement in S/N is also afforded by averaging the signal from the ~1200 pixels in each fiber spot. The 10%–90% rise time indicates that single-shot response time is ~15 ps, limited by the temporal delay between adjacent probe pulses. Additional shots with small changes in the delay line position can increase the point density, allowing realization of a rise time limited by only GVD as described in Sec. III.

Also shown in Fig. 2 is a base line trace, taken with no pump pulse. This clearly shows the level of noise possible ($\sim 2 \times 10^{-3}$ Absorbance units rms) in this experiment in single shots. Some of this noise is due to fiber-to-fiber changes in intensity in the pump and probe shots, which arises from spatial fluctuations in the beam intensity where it enters the fiber. This type of noise is especially apparent when averaging many single shots. It can be corrected for by use of the reference camera, which eliminates the need for consecutive images for signal and reference, as shown in Sec. IV B. Some of this noise may be due to variations in light intensity at the edges of the circular area defined for the signal from each fiber, possibly due to mode beating in the fibers and the speckle apparent in the image in Fig. 1. While not fully understood, it was observed that better S/N was obtained by using a circle to define the fiber that was slightly smaller than the actual image, and that defining circles larger than the fiber images to collect all of the light from them resulted in significantly worse S/N. This may also indicate a source of noise that scales with the number of pixels used, which may include a combination of CCD analog-to-digital conversion noise and dark (thermal) noise, though this is small due to the low detector temperature and short exposure time.

Careful inspection shows that there is a slightly greater amount of apparent noise in the laser dye decay trace than in the base line trace. This is in fact not random noise. If many shots are averaged, the base line noise gets better as one expects, but this additional component remains largely unchanged. Rather, it is due to the differing amount of excitation light overlapped with each fiber in the sample because the pump beam profile is not completely flat, despite significant efforts to make it so. This nonuniformity leads to slightly different amounts of excitation in each probe spot, leading to this additional type of "noise." This effect can be corrected when necessary, as will be shown for pulse radiolysis experiments below.

B. Single-shot detection for pulse radiolysis

The most important application of this detection system in our laboratory is its use to measure transient absorption kinetics following a 7–10 ps electron pulse in pulse radiolysis, rather than a laser pump pulse. Data are collected in the same fashion as described above, but additionally utilizes the reference camera. The reference camera corrects for both shot-to-shot noise due to changes in illumination of the fibers relative to each other, as well as changes in the average probe intensity. The final absorbance measured by light from each fiber is calculated using the intensity data extracted from a total of eight images from the signal and reference cameras, collected in a series of four shots,

$$\mathrm{abs} = -\log\frac{EP_S - E_S}{P_S - D_S} + \log\frac{EP_R - E_R}{P_R - D_R}.$$

Here EP refers to the light intensity from a shot with both the electron and probe pulses, E from a shot with the electron only, P from a probe only shot, and D from a dark shot taken without either electron or probe pulse. The subscripts S and R denote data from signal and reference camera images, respectively. When averaging is employed, it is usually only necessary to recollect the EP and P shots. When the camera temperature is stabilized, the dark shot does not change appreciably, and thus needs to be collected only once. The electron-only shot corrects for a small amount of light on the signal camera due to Cerenkov radiation. Depending on the sample, this shot also accounts for fluorescence and phosphorescence due most commonly to creation of excited states by absorption of Cerenkov, direct energy deposition by the energetic electron as well as charge recombination. These sources of light illuminate the detector fairly uniformly, and thus their time dependences do not contribute to the observed kinetics. As the total light intensity from these sources is small, and furthermore the electron pulse size fluctuations are small, the electron-only shot can also typically be collected only once. This nearly halves the number of electron shots needed when averaging, which is especially important for samples that are damaged by the electron pulse.

Samples are typically placed in sealed 0.5 cm path length fused silica cells. Longer cells can be used, but the time resolution degrades due to the fact that the electron pulse travels at the speed of light in vacuum, while the probe pulse effectively travels slower by the sample's index of refraction. In addition, a 1 cm cell only provides about a 40% larger signal due to scattering of the 8.5 MeV electron beam in the first part of the sample. As noted in the experiment description, for pulse radiolysis experiments the electron pulse is brought through a pellicle mirror before the sample such that it is collinear with the probe pulse to maximize the signal amplitude.

To demonstrate this experiment, a sample of a standard solution containing 20% methanol and 0.1M NaOH in distilled water was degassed with argon. Solvated electrons are produced following ionization of water in much less than 1 ps, and absorb strongly throughout the red region of the spectrum with a long lifetime. The standard solution is used because the solvated electrons produced decay more slowly than in neat water, and the decay kinetics have been very well characterized.[24] Single-shot transient absorption data collected following pulse radiolysis are shown in Fig. 3. These data were collected using the OPA light source, and a probe wavelength of 760 nm. Changes in probe color as the OPA is tuned require refocusing of the probe to maintain sharp bundle images. This can be remotely accomplished without entering the accelerator vault within a single OPA tuning curve (defined by the combination of harmonic and mixing crystals being used), outside which changes in the OPA output can require manual realignment. To obtain better S/N, 25 electron pulse shots were averaged. The rise time of

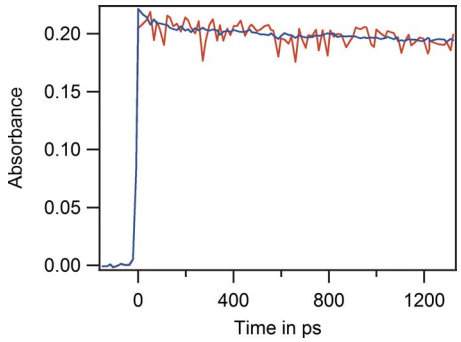

FIG. 3. (Color online) Transient absorption data of solvated electrons at 760 nm in an argon-purged aqueous solution containing 0.1*M* NaOH and 20% methanol. The trace with more apparent noise (red) is an average of 25 shots. The smoother trace (blue) is the same data after correction factors for spatial overlap of the electron beam with the fiber bundle image have been applied.

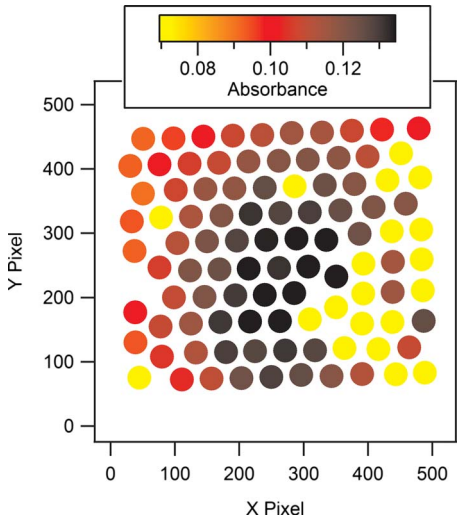

FIG. 4. (Color online) Representation of the fiber bundle image from the signal CCD camera after a single electron pulse from a different data set (with lower dose, at 800 nm) than used in Fig. 3 to accentuate the spatial overlap of the electron beam with the probe. For emphasis, the fiber spots are color coded to indicate the magnitude of the absorbance due to solvated electrons and thus the distribution of dose from the electron beam. The light colored spots (yellow) indicate fibers with delays before the electron pulse, and have an absorbance ~0.

the signal is ~15 ps, consistent with the spacing of the fibers. Unlike the pump-probe experiments described above, shifting the delay line by small amounts to increase the point density will only slightly reduce the apparent rise time, as the electron pulse width of 7–10 ps becomes the limiting factor. The raw signal appears to have considerable noise after time zero. As noted in Sec. IV A, much of this is due to the transverse spatial overlap of the electron pulse with the probe image, which is correctable as can be seen in the corrected data trace and described later. The spatial overlap contribution to the noise in the signal is much larger in pulse radiolysis than was shown for optical excitation because it is necessary to have a reasonably small electron beam to get a large enough signal for good S/N. Consequently, irregularities in the transverse profile of the electron beam are more significant and show up as dose fluctuations and thus absorption differences between fibers.

This effect is quite apparent in Fig. 4, which shows a representation of the data collected by the signal CCD camera after a single electron shot. The data shown are different from that presented in Fig. 3, and were chosen to highlight this effect by using a more tightly focused electron beam. Note also that the electron pulse magnitude was ~1/2 as large in this set of data, compared to that in Fig. 3. For emphasis, each fiber spot is colored to show the magnitude of probe absorption at that location, which is in turn caused by the number of solvated electrons present at each location. The points before time zero have an absorbance of ~0, and are shown as light spots (yellow online). The most intense part of the electron beam is shown with black spots near the center of the array of fibers. As the fiber image in the sample is about 1 mm square, we can deduce from Fig. 4 that the electron beam is close to 2–3 mm in diameter at half maximum. The size of the electron beam spot must be balanced with the signal magnitude; for typical experiments, such as produced the data shown in Fig. 3, the electron beam is usually focused to a larger spot (3–5 mm) than in this picture to give less average absorption but also a relatively smaller amount of fiber-to-fiber signal variation due to overlap. Smaller electron beam diameters can be used, but the larger spatial overlap noise becomes more difficult to correct adequately. This image provides a rough profile of the electron beam, and as such is also very useful during tuning of the electron accelerator. To facilitate this, the data acquisition program continuously updates a picture such as this as a real-time diagnostic to aid in centering and focusing of the electron beam.

In order to correct for the spatial overlap, an independent method is needed to determine the transverse electron beam profile. This is accomplished using the standard solution since its decay is so well characterized and the absorption spectrum of the solvated electron is very broad. Since there is more solvated electron decay in this sample in the first nanosecond than at later times, the delay line is shifted such that the single-shot time window records data at later times where the decay is less pronounced to minimize errors. Time windows starting at 2 ns after time zero work well. A normalized set of multiplicative factors is then determined that relates the observed single-shot data to the known shape of the decay for the solvated electron in this time window. Once determined, these correction factors can be applied to single-shot data collected with any sample, at any time and at any wavelength, as they are simply the ratios of the intensity of the electron beam that overlaps each fiber. In practice the correction factors are not perfect. While there can be small errors due to noise in the data used to generate the correction factors, by far the largest limitation of their usefulness comes from the fact that the electron beam may wander. This motion is fairly small and random on the time scale of seconds, but can result in enough systematic drift after many tens of minutes to significantly reduce the correction factor effectiveness. Such drift could be caused by thermal changes within the accelerator or electron beam transport system. Because of the small amount of beam motion on short time scales, averaging a small number of data sets, typically 25,

produces correction factors that are well representative of the average position of the electron beam. Using a remote sample changer, it is then possible to switch to a different sample as well as move the delay line back to the original position within a few seconds, and collect a set of 25 shots before the electron beam can drift appreciably. It is typically possible to examine multiple samples before the correction factors need to be recollected. The data labeled "corrected data" in Fig. 3 were treated in this manner. It can clearly be seen that the use of such correction factors is very effective at removing structure from the data that are due to spatial overlap of the electron and probe beams. The remaining noise is very close to that in the base line. Correction factors are most necessary for large signals, as the absolute deviations due to spatial overlap grow with the signal magnitude. For small signals, typically less than 5–30 milli-Absorbance units depending on the spatial profile of the electron beam, the base line noise dominates and correction factors are less important.

V. CONCLUSIONS AND OUTLOOK

In this contribution, we have demonstrated a novel type of single-shot transient absorption apparatus based on spatial encoding of temporal information provided by a bundle of different length optical fibers that act as independent and fixed optical delay lines. This system was shown to be useful both for experiments with optical excitation as well as for detection of kinetics following pulse radiolysis. While capable of subpicosecond time resolution, the application to pulse radiolysis is of greatest importance at LEAF, where time resolution is limited only by the electron pulse width. The current optical fiber bundle provides a single-shot time window of ~1.5 ns, which can and has been extended to longer times by shifting the delay of the entire bundle with a standard mechanical delay line. However, one could fabricate a bundle with fibers of nearly any length, making it possible to reach practically any total time window desired. It would also be possible to decrease the differences in length between the shorter fibers which give delays at early times to increase the point density where the signal changes the most rapidly. Such a new bundle with both improvements is currently under construction. The new optical fiber-based instrument is thus a good match for picosecond pulse radiolysis, having a wider and more flexible time window than other ultrafast single-shot techniques while still providing excellent time resolution. This technique has been demonstrated with backilluminated silicon CCD detectors which are sensitive over ~300–1000 nm, however the method could be extended into the near-IR with appropriate InGaAs cameras.

The most important feature of this new equipment is that it enables new pulse radiolysis experiments and projects that were previously impractical or impossible using conventional repetitive variably delayed spectroscopic techniques. These projects utilize a wide range of samples that are too viscous to flow, are solids, or are those available only in extremely limited quantities which are often irreversibly damaged during experiments. Samples as small as 100 μl of such materials are currently under investigation at LEAF to study charge transfer in small molecules and molecular wires, ultrafast charge capture, and primary radiochemical processes in ionic liquids.

ACKNOWLEDGMENTS

The authors would like to thank, in particular, Dr. John Miller for helpful discussions during the development of this experiment, as well as Dr. Jim Wishart, Dr. Sean McIlroy, Dr. Thomas Y. Tsang, and Dr. Peter Z. Takacs. This work was supported by the U.S. Department of Energy, Office of Basic Energy Sciences, Division of Chemical Sciences, under Contract No. DE-AC02-98-CH10886.

[1] G. R. Fleming, *Chemical Applications of Ultrafast Spectroscopy*, International Series of Monographs on Chemistry (Oxford University Press, Oxford, 1986).
[2] M. M. Malley and P. M. Rentzepis, Chem. Phys. Lett. **3**, 534 (1969).
[3] M. R. Topp, P. M. Rentzepis, and R. P. Jones, J. Appl. Phys. **42**, 3415 (1971).
[4] L. Dhar, J. T. Fourkas, and K. A. Nelson, Opt. Lett. **19**, 643 (1994).
[5] J. T. Fourkas, L. Dhar, K. A. Nelson, and R. Trebino, J. Opt. Soc. Am. B **12**, 155 (1995).
[6] R. Weinkauf, L. Lehr, D. Georgiev, and E. W. Schlag, Appl. Phys. B: Lasers Opt. **64**, 515 (1997).
[7] Y. Makishima, N. Furukawa, A. Ishida, and J. Takeda, Jpn. J. Appl. Phys., Part 1 **45**, 5986 (2006).
[8] G. P. Wakeham, D. D. Chung, and K. A. Nelson, Thermochim. Acta **384**, 7 (2002).
[9] G. P. Wakeham and K. A. Nelson, Opt. Lett. **25**, 505 (2000).
[10] P. R. Poulin and K. A. Nelson, Science **313**, 1756 (2006).
[11] G. S. Beddard, G. G. McFadyen, G. D. Reid, and J. R. G. Thorne, Chem. Phys. Lett. **198**, 641 (1992).
[12] I. A. Shkrob, D. A. Oulianov, R. A. Crowell, and S. Pommeret, J. Appl. Phys. **96**, 25 (2004).
[13] D. J. Jang and D. F. Kelley, Rev. Sci. Instrum. **56**, 2205 (1985).
[14] T. Ito, M. Hiramatsu, M. Hosoda, and Y. Tsuchiya, Rev. Sci. Instrum. **62**, 1415 (1991).
[15] J. L. Marignier, V. de Waele, H. Monard, F. Gobert, J. P. Larbre, A. Demarque, and M. B. Mostafavi, Radiat. Phys. Chem. **75**, 1024 (2006).
[16] M. Sakamoto, X. Cai, M. Hara, M. Fujitsuka, and T. Majima, J. Phys. Chem. A **109**, 2452 (2005).
[17] J. F. Wishart, A. R. Cook, and J. R. Miller, Rev. Sci. Instrum. **75**, 4359 (2004).
[18] J. A. Cline, C. D. Jonah, and D. M. Bartels, Rev. Sci. Instrum. **73**, 3908 (2002).
[19] J. W. Goodman and E. G. Rawson, Opt. Lett. **6**, 324 (1981).
[20] C. P. Lin and R. H. Webb, Opt. Lett. **25**, 954 (2000).
[21] D. McMorrow, W. T. Lotshaw, and G. A. Kenney-Wallace, IEEE J. Quantum Electron. **24**, 443 (1988).
[22] A. E. Siegman, *Lasers* (University Science Books, Mill Valley, CA, 1986).
[23] D. J. S. Birch, G. Hungerford and R. E. lmhof, Rev. Sci. Instrum. **62**, 2405 (1991).
[24] D. M. Bartels, A. R. Cook, M. Mudaliar, and C. D. Jonah, J. Phys. Chem. A **104**, 1686 (2000).